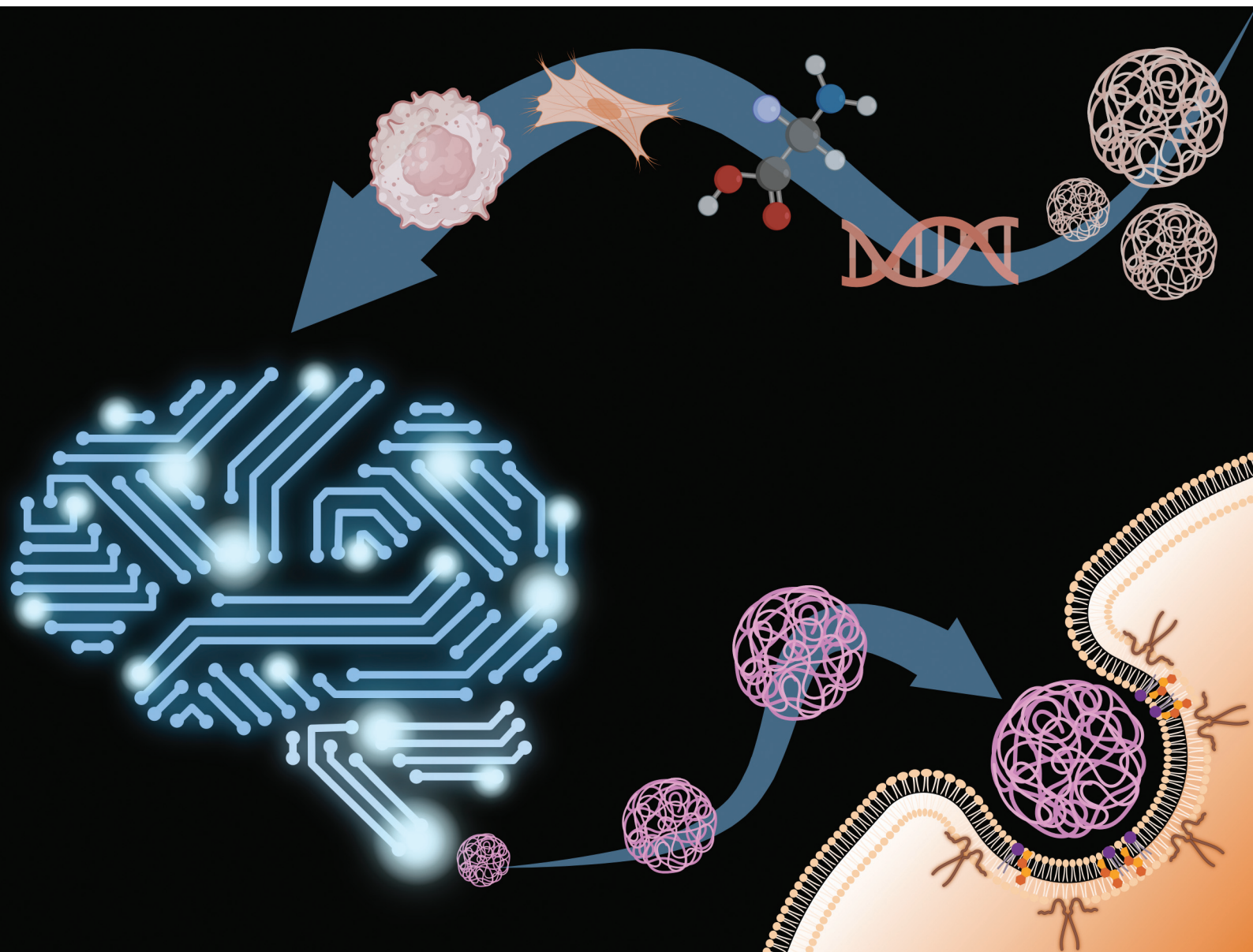


# Biomaterials Science

Volume 11  
Number 17  
7 September 2023  
Pages 5697-6002

rsc.li/biomaterials-science



ISSN 2047-4849



ROYAL SOCIETY  
OF CHEMISTRY

## PAPER

Nuria Oliva *et al.*  
A machine learning approach to predict  
cellular uptake of pBAE polyplexes





Cite this: *Biomater. Sci.*, 2023, **11**, 5797

## A machine learning approach to predict cellular uptake of pBAE polyplexes<sup>†</sup>

Aparna Loecher,<sup>‡</sup> Michael Bruyns-Haylett,<sup>‡</sup> Pedro J. Ballester,<sup>a</sup> Salvador Borros<sup>b</sup> and Nuria Oliva<sup>\*,a,b</sup>

The delivery of genetic material (DNA and RNA) to cells can cure a wide range of diseases but is limited by the delivery efficiency of the carrier system. Poly  $\beta$ -amino esters (pBAEs) are promising polymer-based vectors that form polyplexes with negatively charged oligonucleotides, enabling cell membrane uptake and gene delivery. pBAE backbone polymer chemistry, as well as terminal oligopeptide modifications, define cellular uptake and transfection efficiency in a given cell line, along with nanoparticle size and polydispersity. Moreover, uptake and transfection efficiency of a given polyplex formulation also vary from cell type to cell type. Therefore, finding the optimal formulation leading to high uptake in a new cell line is dictated by trial and error, and requires time and resources. Machine learning (ML) is an ideal *in silico* screening tool to learn the non-linearities of complex data sets, like the one presented herein, with the aim of predicting cellular internalisation of pBAE polyplexes. A library of pBAE nanoparticles was fabricated and the uptake studied in 4 different cell lines, on which various ML models were successfully trained. The best performing models were found to be gradient-boosted trees and neural networks. The gradient-boosted trees model was then analysed using SHapley Additive exPlanations, to interpret the model and gain an understanding into the important features and their impact on the predicted outcome.

Received 30th April 2023,  
Accepted 27th June 2023

DOI: 10.1039/d3bm00741c  
rsc.li/biomaterials-science

## Introduction

Gene therapy (including DNA- and RNA-based therapies) is a promising strategy to treat a wide range of diseases through the transfer of nucleic acids into the cells of a patient,<sup>1</sup> with the goal of modulating gene and protein expression. Non-viral delivery vectors have emerged as a safer, simpler, and more affordable approach to viral vectors, especially for the cytoplasmic delivery of nucleic acids. Moreover, they have no constraint on the size and number of nucleic acid inserts, making them an excellent alternative delivery vector.<sup>2</sup> However, transfection efficiency is typically lower than that observed with viral vectors and is dependent on the physicochemical properties of the nanoparticles and the cell type. This implies that nanoparticle formulations need to be optimised on a case-by-case basis for each specific cell type.

Poly- $\beta$ -amino esters (pBAEs) are highly versatile polymers with amenable chemistry that enable facile tunability of their

physicochemical properties, like polarity, molecular weight, and charge. Their cationic nature enables the electrostatic binding and condensation of negatively charged nucleic acids into nanoparticles.<sup>3</sup> Furthermore, they are biodegradable and biocompatible. Initial high throughput screening of large pBAE libraries (over 2000 formulations) revealed promising polymer structures with efficient transfection in COS-7 cells, an easy-to-transfect cell system useful for high-throughput biological assays.<sup>4</sup> Linear pBAEs with an amine/acrylate ratio of 1.2:1 and terminal secondary amines were found to have much higher cellular uptake and transfection efficiency, as did also those pBAEs forming nanoparticles smaller than 200 nm and near neutral zeta ( $\zeta$ ) potential. While this combinatorial chemistry approach revealed key insights into pBAE-mediated gene-delivery, synthesis of over 2000 polymers is time-consuming and costly. Moreover, the data gathered had no prediction potential and was valid only for the cell line of study. Therefore, knowing which nanoparticle formulation will result in optimal cellular internalisation in each cell line before performing transfection experiments is almost impossible, therefore making it a process of largely trial and error and requiring high amounts of time and resources.<sup>5</sup>

Artificial intelligence (AI), and more concretely its machine learning (ML) branch, can bypass trial and error and be utilised to optimise this process.<sup>5</sup> This is achieved by building ML models that can find trends and predict outcomes by

<sup>a</sup>Department of Bioengineering, Imperial College London, SW7 2AZ London, UK.  
E-mail: nuria.oliva@iqs.ur1.edu

<sup>b</sup>Department of Bioengineering, Institut Químic de Sarrià, Via Augusta 390, 08017 Barcelona, Spain

<sup>†</sup>Electronic supplementary information (ESI) available. See DOI: <https://doi.org/10.1039/d3bm00741c>

<sup>‡</sup>Equal contribution.



exploiting and learning from large, complex, and non-linear data sets. One example are those models built from nanoparticle uptake and transfection data, which are really effective tools for optimising nanomedicine. In fact, the utilisation of ML models to predict nanoparticle behaviour is becoming increasingly widespread. A recent study developed a ML model to predict cellular internalisation of carbon nanoparticles (CNP) in different breast cancer cells. Numerous physicochemical properties of the CNP's were used as inputs to the model, which returned the cellular internalisation as output, minimising the number of nanoparticles needed to be tested *in vitro*. In another study, Damiani *et al.* constructed an ML model to predict the insertion potential of cell-penetrating peptides as delivery vehicles, which could then predict the cellular insertion with high accuracy.<sup>6</sup> A recently published study transfected 488 barcoded cancer cell lines with liposomes, poly(lactic-co-glycolic acid) (PLGA) or polystyrene (PS) nanoparticles and demonstrated that core composition is a key predictor of cell uptake.<sup>7</sup> Moreover, ML revealed that the expression of solute carrier family 46 member 3 (SLC46A3) was inversely correlated with liposome cellular trafficking but had no effect on PLGA and PS uptake and downstream efficacy.

These studies have successfully implemented ML models on various types of nanoparticles and have highlighted the importance of using ML to understand nanoparticle interactions with cells to predict toxicity, uptake, and therapeutic efficiency.<sup>5,6,8</sup> This understanding will pave the way for personalised medicine. To this day, however, there have been no studies using ML for predicting and understanding the cellular internalisation of pBAE nanoparticles. Of special relevance to tissue engineering and regenerative medicine, there is no previous data shedding light on the parameters dictating internalisation in non-cancerous cells. In this work, we have developed a library of pBAE nanoparticles of varying core chemistry, terminal oligonucleotides, and size, and have built and optimised a model of ML as a proof of concept that demonstrates accurate prediction of cellular uptake in a range of cell types (Fig. 1A). With respect to the nanoparticle-related model inputs, our previous expertise demonstrates that the polymer backbone has a large impact on the crossing of the cellular membrane due to variations in polarity caused by the pendant chemical groups: the C6 polymer is more hydrophobic than the C32 polymer<sup>3,9</sup> (Fig. 1B). The addition of terminal oligopeptides composed of basic amino acids such as histidine (H), arginine (R) and lysine (K) (Fig. 1C) also creates different transfection efficiencies based on the type and ratio of oligopeptides.<sup>9,10</sup> Size has also been shown to dictate the cellular uptake of pBAE polyplexes.<sup>4,9</sup>

We have built a proof-of-concept ML model using four distinct cell lines, three cancerous (OVCAR-4, Panc02 and 4T1) and one non-cancerous (Human Dermal Fibroblasts, HDFs). The cancerous cell lines have been chosen based on their characteristics and previous empirical observations. OVCAR-4 and 4T1 have been demonstrated to have overall high levels of uptake across most pBAE formulations. They

are both metastatic cancer cell lines, with OVCAR-4 being an ovarian one of human origin, and 4T1 a breast cancer cell line of murine origin. Panc02 has been explored as 4T1 non-metastatic counterpart (murine pancreatic cancer cell line). Finally, HDFs have been used as a model of non-cancerous cells, which are notoriously harder to transfect using nanoparticles.<sup>3</sup> The three main microscale endocytic pathways through which cells uptake foreign substances are clathrin-, caveolae-, and dynamin-mediated endocytosis,<sup>11</sup> and the uptake route most responsible for transfection can change depending on the pBAE properties, such as size and charge.<sup>12</sup> Additionally, the main endocytic mechanism can vary across different cell lines.<sup>11</sup> Thus, determining the most prevalent mechanisms in each cell type and the preferred mechanism for each nanoparticle is very relevant. For pBAEs, clathrin- and caveolae-mediated endocytosis have been reported as the most prevalent uptake mechanisms.<sup>13</sup> For this reason, we have chosen the normalised expression of genes involved in these pathways as cell-related inputs for the model. Nanoparticle- and cell-related inputs for 60 pBAE formulations and the 4 cell lines described above have been used to train various ML models to establish trends within these inputs and confer the ability to predict the uptake of pBAE polyplexes.

## Materials and methods

### Materials

Reagents and solvents were purchased from Sigma-Aldrich (Spain) and used as received unless otherwise stated. Catalogue number and suppliers are specified next to each chemical in this section. Oligopeptides were purchased from Ontores Biotechnologies Inc. Untagged and 3'-AlexaFluor488 tagged DNA sequences (5'-CCTCAAGTGGGACCATCATAA-[AlexaFluor488]-3') were purchased from IDT (Custom made, UK). Human Dermal Fibroblasts (HDFs) were isolated from adult skin after abdominoplasty procedures, kindly provided by Dr Higgins from Imperial College London. Vials of cancerous cell lines OVCAR-4 (RRID:CVCL\_1627), 4T1 (RRID:CVCL\_0125) and Panc02 (RRID:CVCL\_D627) were provided by Prof. McNeish, Dr Keshavarz and Dr Ishihara, respectively, all from Imperial College London (UK). Products for cell culture (DMEM, RPMI-1640, FBS, phosphate-buffered saline (PBS), glutamine and penicillin-streptomycin solutions, trypsin-EDTA 0.25%) were obtained from Thermo Fisher (UK).

### Cell culture conditions

Panc02 and 4T1 cell lines were cultured in RPMI 1640 Medium (A10491, Thermo Fisher) and OVCAR-4 and HDF cell lines in DMEM (11995, Thermo Fisher). Both media were supplemented with 10% FBS (26140079, Thermo Fisher) and 1% penicillin-streptomycin (15070063, Thermo Fisher). Cells were kept in an incubator at 37 °C and 5% CO<sub>2</sub>. Cells were thawed and passaged using established techniques.



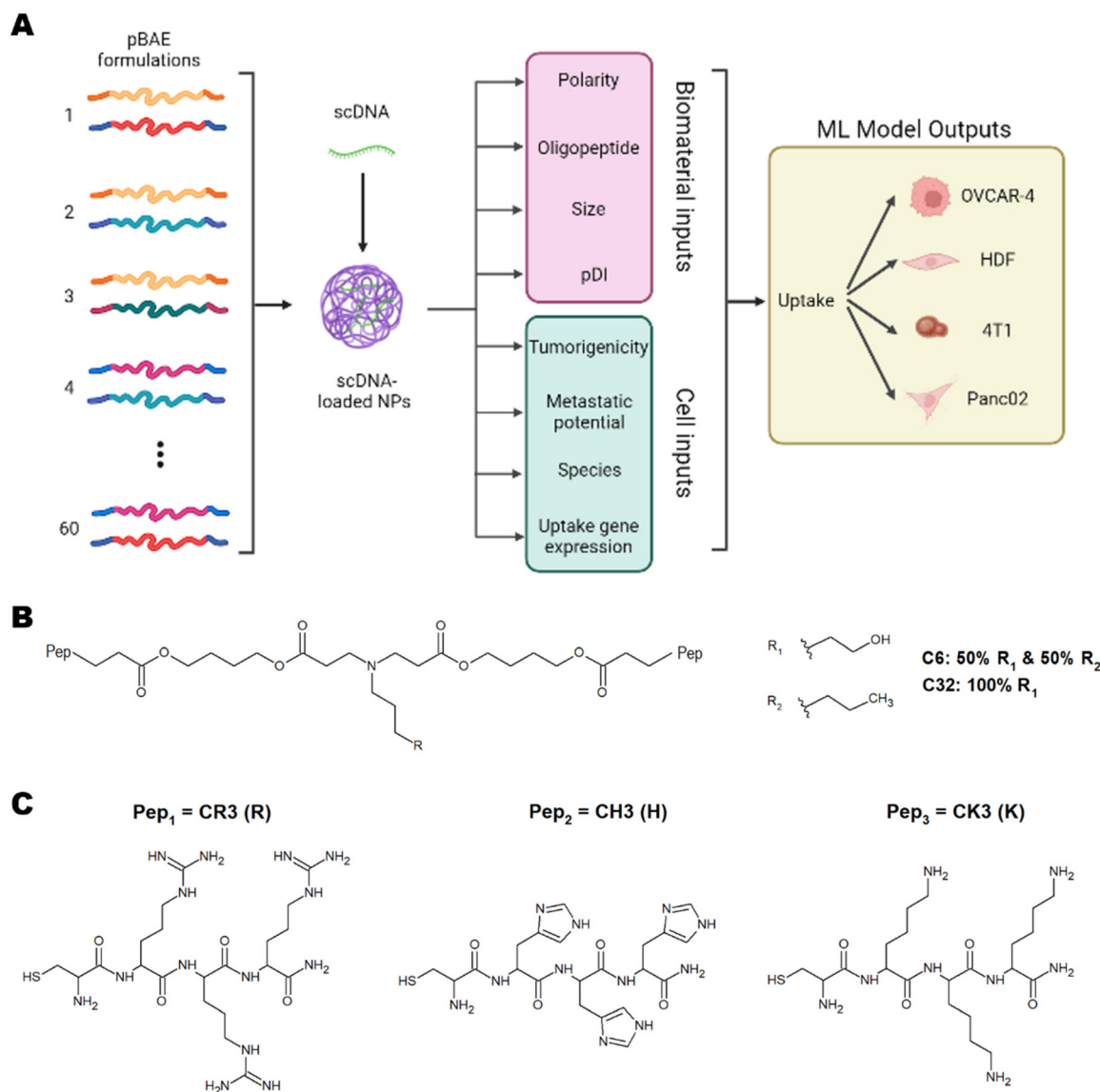


**Fig. 1** (A) Scheme of proposed ML inputs and outputs. Chemical structure of (B) pBAE backbone polymer and (C) terminal oligopeptides arginine (R), histidine (H) and lysine (K). Created with BioRender.com.

### Synthesis of pBAE polymer backbones

Acrylate-terminated poly( $\beta$ -aminoester)s C32 and C6 (Fig. 1B) were synthesised following a procedure previously described in the literature by Dosta *et al.*<sup>10</sup> Specifically, the polymer formation occurs by addition reaction of primary amines with diacrylates. C32 polymer was obtained by stirring 5-amino-1-pentanol (7.7 g, 75 mmol; 123048 Sigma Aldrich) and 1,4-butanediol diacrylate (18 g, 82 mmol; 411744 Sigma Aldrich) together at 90 °C for 20 h. For C6 polymer, 5-amino-1-pentanol (3.9 g, 38 mmol; 123048 Sigma Aldrich) was firstly mixed with 1-hexylamine (3.8 g, 38 mmol; 219703 Sigma Aldrich). Then, 1,4-butanediol diacrylate (18 g, 82 mmol; 411744 Sigma Aldrich) was added to the mixture and heated at 90 °C for 20 h. <sup>1</sup>H-NMR spectra were recorded in a 400 MHz Varian (Varian NMR Instruments, Claredon Hills, IL, USA) and metha-

nol-d<sub>4</sub> was used as solvent unless otherwise stated. Polymer backbones were characterised by <sup>1</sup>H-NMR as described in our previous works,<sup>9,10,14,15</sup> using MestReNova Software v14.3.2 (ESI Fig. 1†).

### Modification of acrylate-ended pBAEs with oligopeptides

Peptides were purchased as trifluoro acetic acid salts. The first step was the substitution of trifluoro acetic acid for hydrochloride as counterions. Generally, oligopeptides (100 mg) were dissolved in HCl 0.1 M (10 mL, 320331 Sigma Aldrich) and frozen at -80 °C for an hour. The solution was then freeze-dried. Oligopeptides used in the present work were Cys-Arg-Arg-Arg (CR3), Cys-His-His-His (CH<sub>3</sub>) and Cys-Lys-Lys-Lys (CK3) (Fig. 1C). Peptides hydrochlorides were reacted with acrylate-ended C32 or C6 polymers following a Michael-type



addition at a pBAE:peptide molar ratio of 1:2.5. PBAEs and peptides were dissolved separately in dimethyl sulfoxide (DMSO, 472301 Sigma Aldrich) at 100 mg mL<sup>-1</sup> concentration. Then, polymer solution was added dropwise to the peptide solution. At this point, triethylamine (471283 Sigma Aldrich) was added to the solution in a peptide:triethylamine molar ratio of 1:8. The mixture was allowed to react at room temperature for 48 h. <sup>1</sup>H-NMR spectra were recorded in a 400 MHz Varian (Varian NMR Instruments, Clarendon Hills, IL, USA) and methanol-d<sub>4</sub> was used as solvent unless otherwise stated. OM-pBAEs were characterised by as described in our previous works,<sup>9,10,14,15</sup> using MestReNova Software v14.3.2 (ESI Fig. 2–4†).

### PBAE polyplexes formulation optimisation

Oligopeptide-modified C6 and C32 pBAE nanoparticles were prepared following protocols based on previous works.<sup>16–18</sup> PBAEs and polynucleotides were kept in stocks at 100 mg mL<sup>-1</sup> in DMSO or 1 mg mL<sup>-1</sup> in nuclease-free water, respectively. First, the DNA:polymer ratio was optimised to ensure all DNA had been encapsulated without compromising cell viability. A model pBAE formulation previously used in the group, called C6RH (C6CR3:C6CH<sub>3</sub> in a 60:40 ratio), was used for optimisation purposes.<sup>3</sup> Polyplexes were formed using a fixed concentration of DNA (0.06 μg μL<sup>-1</sup>) and increasing concentrations of C6RH pBAE at DNA:polymer ratios of 1:25, 1:50, 1:75 and 1:100. Encapsulation efficiency was analysed by agarose gel electrophoresis. Briefly, 10 μL of nanoparticle solution were mixed with 2 μL loading buffer (10816015 Thermo Fisher, UK), loaded onto a gel prepared with 2.5% agarose (AG002 Appleton Woods, UK) in 1× TBE buffer (15581044 Thermo Fisher UK), and run for 30 minutes at 80 V and 400 mA (Mini-Sub Cell GT, 1704406 Bio-Rad). Cell viability was measured with Presto Blue metabolic assay (A13262 Thermo Fisher UK), following established protocols. Fluorescence signal was recorded using a CLARIOstar Plus plate reader.

### Library of PBAE polyplexes for ML model

A library of 60 different pBAE formulations was created by altering the ratios of both the polymer (C6 or C32) and the oligopeptide (R, H or K), as shown in Table 1 on the left. For each formulation, polyplexes were synthesised as previously described, following the optimal pBAE:DNA ratio of 50:1, determined as described above for this particular DNA structure. Briefly, 0.4 μL of pBAE stock solution (100 mg mL<sup>-1</sup> in DMSO) and 0.8 μL scramble DNA solution (1 mg mL<sup>-1</sup> in RNase/DNase free water) were diluted in 12.1 μL and 11.8 μL acetate buffer (12.5 mM, 4.8 pH), respectively. These two solutions were then mixed with a pipette for a few seconds and left at room temperature for 30 min. The resulting nanoparticles could then be used for transfecting cells, dynamic light scattering (DLS) or gel electrophoresis.

### Data collection for ML model

Along with polymer chemical characteristics, measured inputs for the model included size, polydispersity and gene

**Table 1** pBAE formulations used in ML model. The nomenclature is as follows: X<sub>m</sub>/Y<sub>n</sub> – A/B; where X and Y are the type of polymer (C32 or C6), m and n are the terminal oligopeptides (R, K or H) and A and B are the mass percent ratios between the polymers defined by X<sub>m</sub> and Y<sub>n</sub>

Formulation number	Ratio
1	6R/6H – 80/20
2	6R/6H – 60/40
3	6R/6H – 20/80
4	6R/6K – 80/20
5	6R/6K – 60/40
6	6R/6K – 20/80
7	6H/6K – 80/20
8	6H/6K – 60/40
9	6H/6K – 20/80
10	6H – 100
11	6R – 100
12	6K – 100
13	32R/32H – 80/20
14	32R/32H – 60/40
15	32R/32H – 20/80
16	32R/32K – 80/20
17	32R/32K – 60/40
18	32R/32K – 20/80
19	32H/32K – 80/20
20	32H/32K – 60/40
21	32H/32K – 20/80
22	32H – 100
23	32R – 100
24	32K – 100
25	32R/6H – 80/20
26	32R/6H – 60/40
27	32R/6H – 40/60
28	32R/6H – 20/80
29	32R/6R – 80/20
30	32R/6R – 60/40
31	32R/6R – 40/60
32	32R/6R – 20/80
33	32R/6K – 80/20
34	32R/6K – 60/40
35	32R/6K – 40/60
36	32R/6K – 20/80
37	32H/6H – 80/20
38	32H/6H – 60/40
39	32H/6H – 40/60
40	32H/6H – 20/80
41	32H/6R – 80/20
42	32H/6R – 60/40
43	32H/6R – 40/60
44	32H/6R – 20/80
45	32H/6K – 80/20
46	32H/6K – 60/40
47	32H/6K – 40/60
48	32H/6K – 20/80
49	32K/6H – 80/20
50	32K/6H – 60/40
51	32K/6H – 40/60
52	32K/6H – 20/80
53	32K/6R – 80/20
54	32K/6R – 60/40
55	32K/6R – 40/60
56	32K/6R – 20/80
57	32K/6K – 80/20
58	32K/6K – 60/40
59	32K/6K – 40/60
60	32K/6K – 20/80

expression, to predict the cellular uptake as model output. All experimental data for the model can be found in GitHub (<https://github.com/mbhaylett23/pBAE-cellular-uptake-ML>).



**Size and polydispersity.** Analysis of particle size distribution was performed in a Nanosizer ZS instrument (Malvern Instruments, UK) diluting polyplexes in a 10-fold volume of phosphate-buffered saline (PBS 1×). Data was analysed using ZS Xplorer (v3.2.2).

**Cellular uptake.** To determine cellular uptake, fluorescently labelled DNA was mixed with non-fluorescent DNA at a 1 : 10 ratio, and encapsulated in the polyplexes to enable fluorescence tracking. Cells (OVCAR-4, 4T1, Panc02 or HDF) were seeded in a 96-well plate at a density of 10 000 cells per well, and incubated for 24 hours at 37 °C. Polyplexes containing 10% fluorescent DNA were mixed with non-supplemented DMEM in a 1 : 10 ratio, to reach a final concentration of 0.003 µg µl<sup>-1</sup> DNA in each well, and 100 µL of the nanoparticle medium was added into each well and incubated at 37 °C for 3 hours. The media was then exchanged to supplemented DMEM. In total, each cell line was transfected with 60 different formulations, performing duplicates for each one. The cells were then detached and the fluorescence intensity per cell was measured in duplicate for each well, using a Countess 3 FL fluorescence cell counter. This gave 4 uptake measurements to average for each formulation in every cell line. Gating conditions were determined using untreated controls, with intensities below 97 RFU being considered background (ESI Fig. 5A–C†).

**Gene expression.** Agilent whole genome microarray data for each cell line of interest was downloaded from Gene Expression Omnibus database (GEO Accession Numbers GSM1406256, GSM1529765, GSM564167 & GSM613188). Matlab Microarray Data Normalisation and Filtering Toolbox was used to normalise gene expression data for all cell lines, after which normalised mean signals for a subset of 6 genes involved in clathrin- or caveolae-mediated endocytosis were extracted and used in the ML models. Matlab version used was 9.14.0.2206163 (R2023a).

## Modelling

All modelling was performed in Python (v3.10.10) – the code can be found on GitHub: (<https://github.com/mbhaylett23/pBAE-cellular-uptake-ML>). Overall, the models that were created included multi-linear regression (LM), random forests (RF), gradient-boosted trees (GBT) and neural networks (NN). For all models, feature normalisation was performed on the data, and the data was split into training, validation and test sets in an 80 : 10 : 10 ratio using the scikit-learn (v1.2.2) library. The models were trained on the training set, tuned on the validation set and then evaluated on the test set. Performance of the models was evaluated by calculating the mean absolute error (MAE) between the model's uptake prediction and the actual uptake. The MAE is the average absolute difference between the predicted and observed outputs, and is useful for assessing the performance of a model on a particular dataset.<sup>19</sup>

**Multi-linear regression (LM).** The multi-linear regression model was created using linear regression algorithms from the scikit-learn (v1.2.2) package.

**Tree-based models.** The two types of tree-based models built and trained were a random forest (RF) and a gradient-boosted trees (GBT) model. These were created using algorithms from the scikit-learn package. Both models were tuned to find the best hyper-parameters using a grid search algorithm. In these searches the depth of each tree was varied between 5–25, and the number of trees was varied between 50 and 300.

**Deep neural network (NN).** The NN model was created using Keras (v2.10.0), a deep learning package. A sequential model was built, with an input layer, hidden layers and output layer. The input layer had 9 nodes and the output layer had one node. The activation function used in the hidden layers was the ReLU, due to its computational efficiency. To train the model, 100 epochs were run. During tuning, the batch size used for training was varied between 1–10. The number of hidden layers and nodes in each hidden layer were varied between 1–3 and 5–90 respectively. Both were kept relatively small due to the small training set. Different optimisers including RMSprop and ADAM were also implemented to find the best resulting performance. To find the optimal hyper-parameters, the KerasTuner library RandomSearch was implemented.

## Statistical analysis

All statistical analyses of data were performed with the GraphPad Prism software (v9.5.1), using ANOVA (analysis of variance) tests (one-way and two-way) unless stated otherwise. Statistical significance was calculated based on  $p \leq 0.05$ , where \*, \*\*, \*\*\* and \*\*\*\* represent  $p \leq 0.05$ ,  $p \leq 0.01$ ,  $p \leq 0.001$  and  $p \leq 0.0001$ , respectively.

## Results and discussion

### Optimisation of DNA : polymer ratio

Four different DNA-to-pBAE proportions (1 : 25, 1 : 50, 1 : 75 and 1 : 100) were synthesised and analysed for encapsulation efficiency and cytotoxicity. The DNA was completely encapsulated at DNA : pBAE ratios of 1 : 50 and higher (ESI Fig. 6A†), as evident by the disappearance of the free DNA band in gel electrophoresis. No statistically significant cytotoxicity was observed for any formulation except the 1 : 100 ratio (ESI Fig. 6B†). Therefore, for the rest of this study, a DNA : pBAE ratio of 1 : 50 was used.

### Nanoparticle size and polydispersity

The measurements of the sizes (Fig. 2A) and polydispersities (Fig. 2B) of all 60 formulations presented statistically significant variations ( $p < 0.0001$  for both One-Way ANOVAs). The sizes ranged between 58 and 694 nm in diameter, and the polydispersities between 0.01 and 0.737. In general formulations with high amounts of C6K and C32H tend to result in



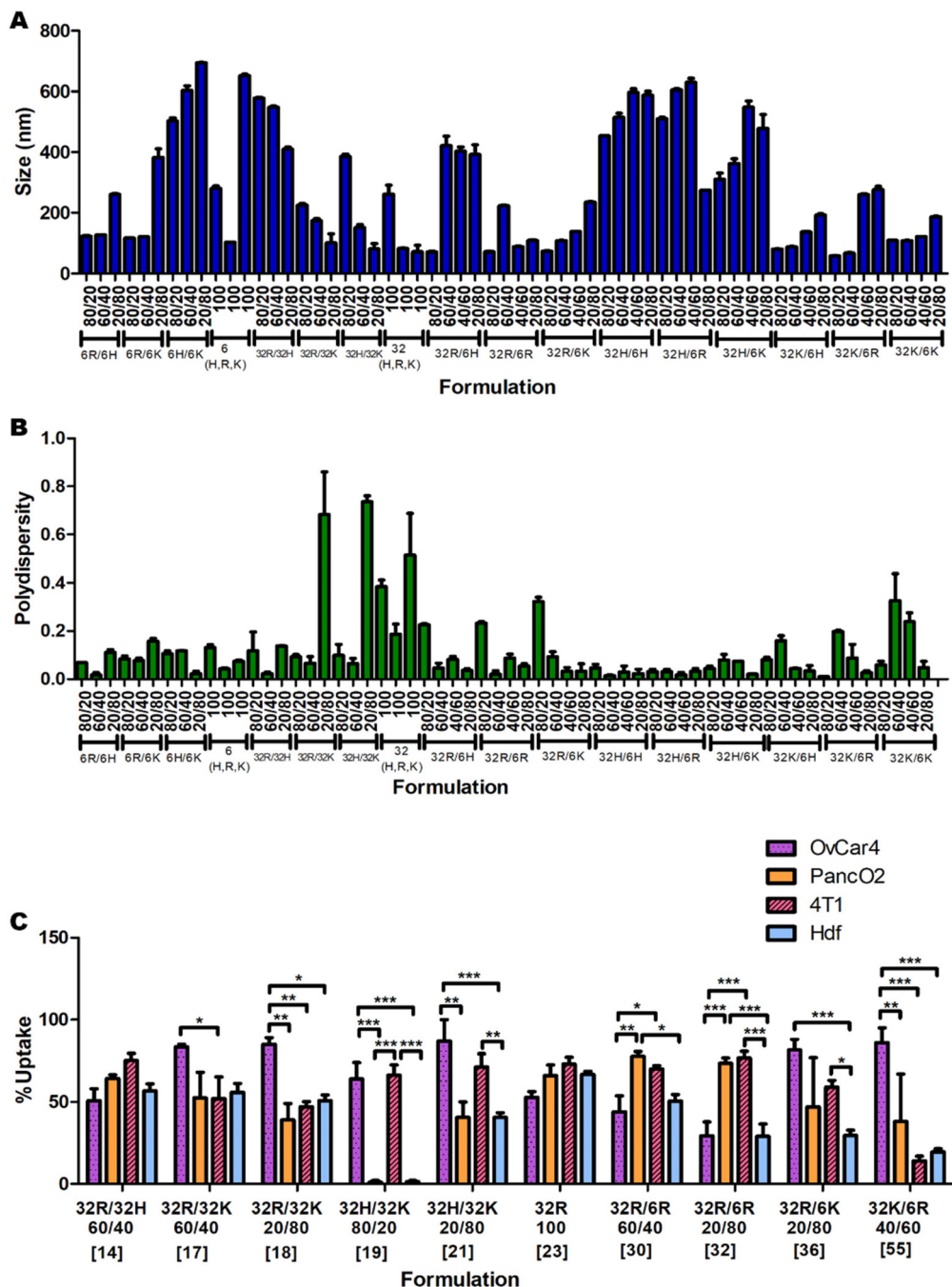


**Fig. 2** Nanoparticles (A) size and (B) polydispersity for 60 pBAE formulations of various ratios of polymer backbone chemistry and terminal oligopeptides. (C) A summary of cellular uptake of 10 of the 60 formulations in the four cell lines of study (OVCAR-4, 4T1, PancO2 and HDF) presents no clear trend.

larger sizes, and formulations with high amounts of C32K tend to result in higher polydispersity.

### Cellular uptake of nanoparticles

The uptake of the 60 nanoparticle formulations was measured in OVCAR-4, HDF, 4T1 and Panc-02 cell lines (ESI Fig. 7A, B and 8A, B†). A summary of a few significant formulations is shown in Fig. 2C to demonstrate the apparent unpredictability

of the system and confirm the hypothesis that tuning the backbone polymer and the oligopeptide ratios affects the cellular uptake. Additionally, there is variation in the amount of uptake for specific nanoparticles between different cell lines. For instance, formulation 19 has medium-to-high transfection efficiency in OVCAR-4 and 4T1, but almost-zero uptake in PancO2 and HDF. However, formulation 32 has high uptake in PancO1 and 4T1 cells, and low cellular entry in OVCAR-4 and



HDF. Each cell line was found to have a different formulation that resulted in the highest uptake: for OVCAR-4 it was formulation 21, with 87% uptake, for 4T1 it was formulation 31, with 83%, for Panc02 it was formulation 30, with 77% and for HDF it was formulation 23, with 66% uptake.

Predicting which formulation would have resulted in the highest uptake in each cell line without a ML model would have been impossible, showing the need for a predictive model. Another interesting observation is that the cancer cell lines all had a higher average uptake than the non-cancerous cell line. The average uptakes of OVCAR-4, 4T1, Panc02 and HDF were 44%, 40%, 29% and 23% respectively. The trend that cancer cells have higher uptake of various types of nanoparticles has been reported in the literature.<sup>20</sup> This is mostly because cancer cells consistently undergo endocytosis more rapidly than noncancerous cells, to provide themselves with more nutrients.<sup>21</sup> This highlights the importance of ML models to maximise uptake and transfection in non-cancerous cells and enable this way the use of pBAE polyplexes in regenerative medicine. Within cancer cells, metastatic ones (OVCAR-4 and 4T1) present higher average uptake than non-metastatic Panc02 (44 and 40% *versus* 29%, respectively). To further understand the effect of the cell type on uptake and provide additional prediction capability to the model, we investigated the expression of key genes involved in polyplexes' uptake and cell trafficking.

### Gene expression

It has been previously described in the literature that there is a preferential uptake of polyplexes into cells through clathrin- and caveolae-mediated endocytosis.<sup>13</sup> More interestingly, previous studies using pBAEs demonstrated that altering the polymer backbone chemistry and terminal groups preferentially triggered one pathway over the other.<sup>12,22</sup> Therefore, incorporating the expression of key genes regulating these cellular trafficking pathways is a promising approach to improve the prediction capability of the ML model. The expression of genes involved in clathrin- and caveolae-mediated endocytosis (Fig. 3A) were extracted from publicly available microarray data and normalised to the total microarray intensity (Fig. 3B) prior to data input in the models. Interestingly, the expression of these genes is significantly different in the four cell lines of study, and overall there seems to be an overexpression of genes involved in clathrin-mediated endocytosis and underexpression of caveolae-related genes.

### Initial data analysis

Some initial data analysis on the experimental uptake data was performed to discover trends. Pure formulations (only one type of polymer) were evaluated first (Fig. 4). In all cell lines, polymers C6H and C32H resulted in approximately zero uptake (Fig. 4A and B). Additionally, given the oligopeptide terminal R or K, the C32 backbone results in higher uptake than the C6 backbone across all cell lines. Lastly, OVCAR-4 seems to have the highest affinity to C32K, while 4T1, Panc02 and HDF have the highest affinities to C32R.

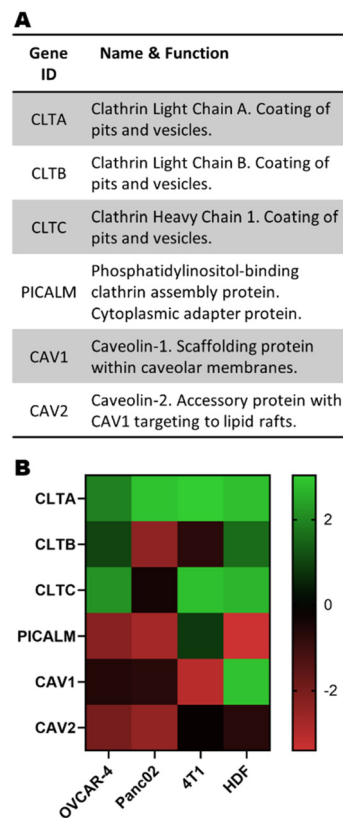
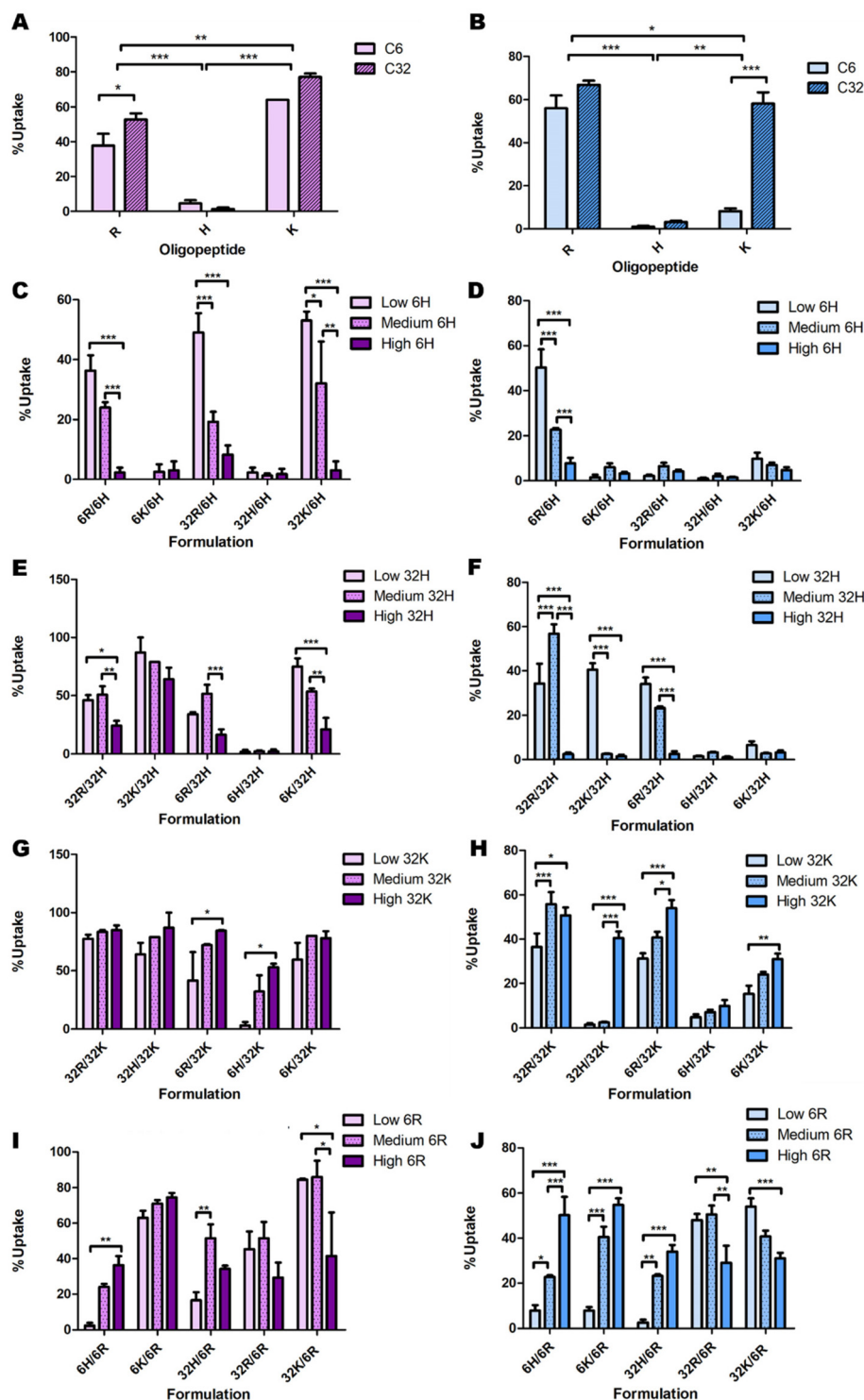


Fig. 3 (A) Subset of genes linked to clathrin- and caveolae-mediated endocytosis and (B) their normalised expression.

Delving further into these trends, the data point to a consistent decrease in nanoparticle uptake as the percentage of C6H and C32H increase (Fig. 4C–F & ESI Fig. 9†). However, there are a few exceptions in which 60% C32H (referred to as “medium” amounts in the corresponding graphs) increase the uptake (Fig. 4E and F). This is explained by the endocytic process leading to transfection. To efficiently deliver the genetic material, endosomal escape of the particles must occur after uptake. The process called ‘proton sponge effect’ facilitates endosomal escape, and is driven by terminal amines with high buffering capacity.<sup>9</sup> Histidine has the highest buffering capacity, making it the best for inducing endosomal escape inside cells. However, this study focuses only on cellular uptake, without considering the ability to successfully transfect cells (which would include endosomal escape). Since high transfection has been found to be a result of high cellular uptake, rather than high endosomal escape,<sup>9</sup> we focused on this first as a proof-of-concept study on cellular uptake only. Thus, while histidine decreases cellular uptake, and might seem dispensable in this system, including minimal amounts of histidine in the formulation will have an impact on overall transfection efficiency through increased endosomal escape.

A similar analysis on C6K revealed inconclusive trends (ESI Fig. 8C and D†). While C32K effects on Panc02 and 4T1 cell lines were also inconclusive (ESI Fig. 8E and F†), OVCAR-4 and HDF seem to follow a trend with higher uptake as the amount





**Fig. 4** Initial analysis of the effects of backbone chemistry and terminal oligopeptide on cellular uptake in OVCAR-4 (A, C, E, G & I; purple bars) and HDF (B, D, F, H & J; blue bars), both for (A and B) pure formulations and low, medium and high ratios of (C and D) C6H, (E and F) C32H, (G and H) C32K and (I and J) C6R. The remaining combinations presented no clear trends (Fig. S4 and S5<sup>†</sup>).

of C32K increases (Fig. 4G and H). Interestingly, HDFs had low affinity for pure C32K. This suggests that mixing polymers and oligopeptides results in completely different interactions with cells. Finally, there is no conclusive trend in C6R and C32R

uptake (Fig. 4I and J & ESI Fig. 10A–F<sup>†</sup>). However, medium amounts of 6R result in higher uptake in most formulations in OVCAR-4, Panc02 and 4T1 cell lines, while uptake trends are inconclusive in HDF.



Overall, while a few trends can be observed, complex non-linear relationships at play exist that are not obvious. This further highlights the need for a model to learn these complexities and accurately predict which formulations result in high uptake in a certain cell line.

### Model results

After creating and tuning the four different models to have low MAE (ESI Fig. 10A†), and balance bias and variance, the optimal hyper-parameters are shown in Table 2. MAE values showed GBT was the best performing model, followed by the NN model and the RF model, with multi-linear regression (LM) performing the most poorly. Non-linear ML models GBT and NN have statistically significant decreases in MAE compared to multi-linear regression (ESI Fig. 11†). Both the GBT and NN models have statistically non-significantly different mean performances, with an MAE of 10.57 and 11.17, respectively, about 30% better than that of the multi-linear regression model. This shows that the uptake data and its corresponding features have complex non-linearities, from which ML models are able to learn from and better capture trends.

### SHAP (shapley additive exPlanations) analysis

A model that returns good predictions is useful, however, if there is no understanding as to how the model uses the inputs to make its predictions, it can be of limited use. The SHAP approach gives an understanding of both the contributions of the features globally, as well as contributions for individual observations.<sup>23</sup> This renders the ‘black box’ ML model interpretable and is especially relevant here, because understanding the importance of each feature can help in the design process of the nanoparticles. Since the GBT and NN models had the best performance overall, and calculating SHAP-values for GBT was computationally more efficient than for the NN, SHAP analysis was implemented on the GBT model.

**Global explanations.** The global importance of each feature in the model is shown in Fig. 5A. The most important feature is C6H, due to high percentages of C6H leading to zero uptake, thus making it a very determining factor. Size is the second most important feature, which has already been described in previous studies.<sup>4</sup> C32R and C32H are also very important in determining the uptake. Interestingly, the positions 5 to 7 in global importance are monopolised by cell-



**Fig. 5** SHAP analysis of model data. (A) Overall importance of each feature on the model output, and (B) Influence of each feature value on the model output.

related inputs, highlighting the cell-dependent variation in uptake and the need for an ML model. In particular, expression of CLTA and PICALM have an important effect on the model output, which aligns with previous observations that pBAE nanoparticles enter cells through clathrin-mediated endocytosis.<sup>12,22</sup> On the other hand, and despite previous studies reporting caveolae-mediated endocytosis as an alternative uptake mechanism triggered by certain formulations,<sup>13</sup> expression of CAV1 and CAV2 have minimal impact on the model output (positions 13 and 17 out of 17 inputs and mean SHAP values close to 0). Finally, the cells' species (human or murine) has minimal impact on the model output (position



14 of 17 and mean SHAP value close to 0). The power of understanding the model with these SHAP-values is evident: the results directly informed a training set modification that can be utilised in the future.

A more in-depth explanation of how the specific value of each feature contributes to the model output is depicted in Fig. 5B. High negative SHAP-values mean that features greatly decrease the uptake, while highly positive SHAP-values mean that features strongly increase the uptake. For C6H, C32H and C6K, high percentages result in high negative SHAP-values and *vice versa*. This trend was observed in initial data analysis in Fig. 4. High amounts of C32R and C6R lead to higher model outputs and *vice versa*, while C32K displays no clear trend. Overall, as size values are lower, there is a high positive impact on the output of the model, which is in line with research having shown that optimal sizes of nanoparticles that enter most cells endocytically are between 100–200 nm.<sup>4,9</sup>

In terms of the cell type and phenotype, high expression of CLTA results in low model output, while high levels of PICALM lead to high model outputs. This seems contradictory, as both genes are part of the same clathrin-mediated endocytosis pathway. Interestingly, while high expression of CLTA (pink dots) has a consistent negative impact on the model output, low levels (blue dots) might have a positive or negative impact on uptake. Similarly, high PICALM expression consistently improves uptake, while low levels can lead to either high or low model output. These data suggest that the expression of clathrin-mediated genes is key for some formulations, but not for others, as previously described.<sup>12,22</sup> A more in depth, partial dependence investigation delves into these findings in the next section. Lastly, metastatic cells display higher levels of uptake than non-metastatic cells, while tumorigenicity and species (human or murine) have no impact on the model outputs. Overall, this SHAP analysis shows that the model has consistently been able to learn the trends initially observed.

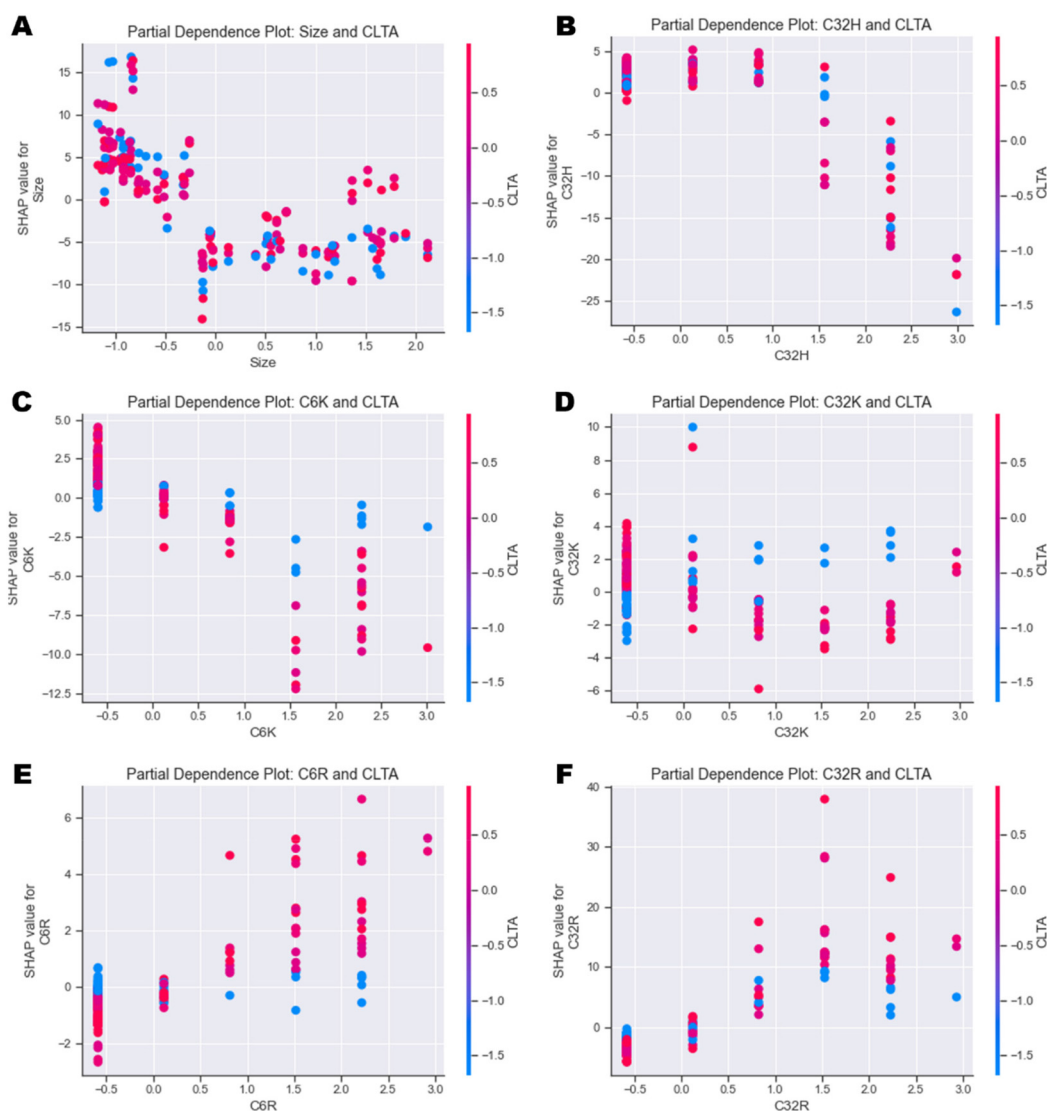


**Fig. 6** Partial dependence plots investigating the individual feature interactions between CLTA expression and (A) Size, (B) C32H, (C) C6K, (D) C32K, (E) C6R and (F) C32R.



**Feature interactions.** To go into more depth regarding the impact of each feature on every cell line, further SHAP analysis allowed for the creation of partial dependence plots, which show the interaction of two variables on the predicted output (Fig. 6 and ESI Fig. 12 & 13†).

In general, the output of the model decreases as size increases independently of the cell type (Fig. 6A and ESI Fig. 12A†). Similarly, high values of C32H and C6H also have a negative impact on uptake independently of cell type (Fig. 6B and ESI Fig. 12B–D†). Partial dependence plots of arginine (R) and lysine (K) polymers *versus* CLTA and PICALM reveal very interesting correlations. Presence of C6K and C32K leads to higher uptake in those cells with lower expression of CLTA (Fig. 6C & D), while C6R and C32R triggered higher uptake in cells expressing high levels of CLTA (Fig. 6E & F). This suggests that polymers with terminal arginines potentially use clathrin-mediated endocytosis. PICALM dependence plots show similar trends: C6K and C32K display higher uptake in those cells with low PICALM expression (ESI Fig. 12E & F†) while C6R and C32R result in higher uptake in cells with higher PICALM levels (ESI Fig. 12G & H†). Finally, further feature interaction analysis shows that C32K polyplexes have higher affinity to metastatic cells, while C6K, C6R and C32R present no clear trend (ESI Fig. 13A–D†), which had already been identified in Fig. 4.

## Conclusions

In summary, data relating to the size, polydispersity and uptake of 60 different nanoparticle formulations in 4 cell lines were collected. Biomaterial and cellular inputs were used to successfully train various ML models to predict the cellular uptake in these cell lines. It is important to highlight that despite the relatively low number of data points (240 uptake values compared to 1000s of points typically used for ML), the SHAP analysis carried out on the GBT model showed that it was successfully able to learn many trends seen in the data. In the future, new cells lines will be investigated to continue to grow the training and validation sets of the model, improving accuracy and reducing MAE.

Aspects like polyplex size, backbone chemistry and terminal oligopeptides play distinct roles in cellular uptake, which often display divergent behaviour in different types of cell lines. Using an ML model approach, we have also identified two genes in the clathrin-mediated endocytosis pathway, CLTA and PICALM, which seem to play a key role controlling cellular trafficking as a function mainly of the identity of the terminal oligopeptides. The data suggests that high expression of these genes makes cells more receptive to the uptake arginine polymers (C6R and C32R), while low levels of these genes trigger the uptake of lysine polymers (C6K and C32K). Histidine is an important feature of the model because high percentages of histidine polymers abrogate the cellular uptake, which explains the lack of any partial dependence with CLTA or PICALM.

This proof-of-concept study demonstrates that ML is a key tool to gain in depth understanding of the complex non-linearities underlying pBAE cellular uptake. This work has been a step towards the ultimate goal of being able to use a model to scan across a number of nanoparticle formulations in a new cell line and predict those with the highest transfection efficiency.

## Author contributions

AL curated the data and performed formal analysis, MBH carried out formal analysis and validation, PJB and SB provided supervision and project administration, NO conceptualised the project, acquired funding and carried out project administration and supervision. AL, MBH and NO wrote the original draft, all authors reviewed and edited the manuscript.

## Conflicts of interest

There are no conflicts to declare.

## Acknowledgements

We would like to thank Prof. McNeish, Dr Keshavarz, Dr Ishihara and Dr Higgins for providing the cells for the study. NO acknowledges an Imperial College Research Fellowship, a Royal Society Research Grant (ID: RGS\R2\212038) and a 'la Caixa' foundation Junior Leader Fellowship (ID: LCF/BQ/PR22/11920009).

## References

- 1 J. A. Kulkarni, D. Witzigmann, S. B. Thomson, S. Chen, B. R. Leavitt, P. R. Cullis, *et al.*, The current landscape of nucleic acid therapeutics, *Nat. Nanotechnol. Nat. Res.*, 2021, **16**, 630–643.
- 2 I. Roy, M. K. Stachowiak and E. J. Bergey, Nonviral gene transfection nanoparticles: function and applications in the brain, *Nanomedicine*, 2008, **4**, 89–97.
- 3 J. A. Duran-Mota, J. Q. Yani, B. D. Almquist, S. Borrós and N. Oliva, Polyplex-Loaded Hydrogels for Local Gene Delivery to Human Dermal Fibroblasts, *ACS Biomater. Sci. Eng.*, 2021, **7**(9), 4347–4361.
- 4 J. J. Green, R. Langer and D. G. Anderson, A combinatorial polymer library approach yields insight into nonviral gene delivery, *Acc. Chem. Res.*, 2008, **41**, 749–759.
- 5 M. Alafeef, I. Srivastava and D. Pan, Machine Learning for Precision Breast Cancer Diagnosis and Prediction of the Nanoparticle Cellular Internalization, *ACS Sens.*, 2020, **5**(6), 1689–1698.
- 6 S. A. Damiati, A. L. Alaofi, P. Dhar and N. A. Alhakamy, Novel machine learning application for prediction of mem-



- brane insertion potential of cell-penetrating peptides, *Int. J. Pharm.*, 2019, **567**, 118453.
- 7 N. Boehnke, J. P. Straehla, H. C. Safford, M. Kocak, M. G. Rees, M. Ronan, *et al.*, Massively parallel pooled screening reveals genomic determinants of nanoparticle delivery, *Science*, 2022, **377**(6604), eabm5551.
  - 8 N. Boehnke and P. T. Hammond, Power in Numbers: Harnessing Combinatorial and Integrated Screens to Advance Nanomedicine, *JACS Au*, 2022, **2**(1), 12–21.
  - 9 N. Segovia, P. Dosta, A. Cascante, V. Ramos and S. Borrós, Oligopeptide-terminated poly( $\beta$ -amino ester)s for highly efficient gene delivery and intracellular localization, *Acta Biomater.*, 2014, **10**(5), 2147–2158.
  - 10 P. Dosta, V. Ramos and S. Borrós, Stable and efficient generation of poly( $\beta$ -amino ester)s for RNAi delivery, *Mol. Syst. Des. Eng.*, 2018, **3**(4), 677–689.
  - 11 S. Kumari, S. Mg and S. Mayor, Endocytosis unplugged: Multiple ways to enter the cell, *Cell Res.*, 2010, **20**, 256–275.
  - 12 J. Kim, J. C. Sunshine and J. J. Green, Differential polymer structure tunes mechanism of cellular uptake and transfection routes of poly( $\beta$ -amino ester) polyplexes in human breast cancer cells, *Bioconjugate Chem.*, 2014, **25**(1), 43–51.
  - 13 J. Rejman, A. Bragonzi and M. Conese, Role of clathrin- and caveolae-mediated endocytosis in gene transfer mediated by lipo- and polyplexes, *Mol. Ther.*, 2005, **12**(3), 468–474.
  - 14 P. Dosta, N. Segovia, A. Cascante, V. Ramos and S. Borrós, Surface charge tunability as a powerful strategy to control electrostatic interaction for high efficiency silencing, using tailored oligopeptide-modified poly( $\beta$ -amino ester)s (PBAEs), *Acta Biomater.*, 2015, **20**, 82–93.
  - 15 N. Segovia, M. Pont, N. Oliva, V. Ramos, S. Borrós and N. Artzi, Hydrogel doped with nanoparticles for local sustained release of siRNA in breast cancer, *Adv. Healthcare Mater.*, 2014, **4**(2), 271–280.
  - 16 P. Dosta, N. Segovia, A. Cascante, V. Ramos and S. Borrós, Surface charge tunability as a powerful strategy to control electrostatic interaction for high efficiency silencing, using tailored oligopeptide-modified poly( $\beta$ -amino ester)s (PBAEs), *Acta Biomater.*, 2015, **20**, 82–93.
  - 17 N. Segovia, P. Dosta, A. Cascante, V. Ramos and S. Borrós, Oligopeptide-terminated poly( $\beta$ -amino ester)s for highly efficient gene delivery and intracellular localization, *Acta Biomater.*, 2014, **10**(5), 2147–2158.
  - 18 P. Dosta, V. Ramos and S. Borrós, Stable and efficient generation of poly( $\beta$ -amino ester)s for RNAi delivery, *Mol. Syst. Des. Eng.*, 2018, **3**(4), 677–689.
  - 19 H. H. Rashidi, S. Albahra, S. Robertson, N. K. Tran and B. Hu, Common statistical concepts in the supervised Machine Learning arena, *Front. Oncol.*, 2023, **13**, 1130229.
  - 20 K. Bromma, A. Bannister, A. Kowalewski, L. Cicon and D. B. Chithrani, Elucidating the fate of nanoparticles among key cell components of the tumor microenvironment for promoting cancer nanotechnology, *Cancer Nanotechnol.*, 2020, **11**(1), 8.
  - 21 D. Wang, S. Liu and G. Wang, Establishment of an Endocytosis-Related Prognostic Signature for Patients With Low-Grade Glioma, *Front. Genet.*, 2021, **12**, 709666.
  - 22 J. C. Sunshine, D. Y. Peng and J. J. Green, Uptake and transfection with polymeric nanoparticles are dependent on polymer end-group structure, but largely independent of nanoparticle physical and chemical properties, *Mol. Pharm.*, 2012, **9**(11), 3375–3383.
  - 23 S. M. Lundberg, G. Erion, H. Chen, A. DeGrave, J. M. Prutkin, B. Nair, *et al.*, From local explanations to global understanding with explainable AI for trees, *Nat. Mach. Intell.*, 2020, **2**(1), 56–67.

